Hindawi
Advances in Civil Engineering
Volume 2022, Article ID 2161744, 14 pages
https://doi.org/10.1155/2022/2161744

Research Article

Model Test and Numerical Simulation Study on the Effect of Mudcake and Length-Diameter Ratio on the Bearing Capacity of Bored Cast-in-Place Piles

Peisheng Xi, Mengxuan Kan, and Yang Liu

Anhui Province Engineering Technology Research Center of Urban Construction and Underground Space, Anhui Jianzhu University, Hefei 230601, China

Correspondence should be addressed to Yang Liu; liuyang880205@126.com

Received 6 May 2022; Revised 8 July 2022; Accepted 16 September 2022; Published 3 October 2022

Academic Editor: Qian Chen

To study the effect of length-diameter ratio and mudcake on the bearing capacity of bored cast-in-place piles, the indoor model test and finite element numerical simulation method were used to carry out the loading test of piles under different mudcake thicknesses (0 and 0.5 mm) and different length-diameter ratios (10, 14, and 24). The variation law of pile top displacement, pile bearing capacity, pile axial force, and lateral friction resistance under the vertical load was analyzed. The results show that the larger the length-diameter ratio of bored pile is, the more effectively the negative influence of mudcake around the pile on the settlement and end resistance of the pile is restrained, and the ultimate bearing capacity of the pile is improved. The research results have important scientific value and practical significance for understanding the influence of length-diameter ratio on bearing capacity of bored cast-in-place piles.

1. Introduction

Due to the advantages of small construction vibration, large bearing capacity, and good seismic performance, bored cast-in-place pile has become a common foundation form for infrastructure such as high-rise buildings and elevated bridges. Both engineering practice and field test show that the bearing capacity of cast-in-place piles is affected by the relevant modifiers [1], but the bearing capacity of cast-in-place piles is still the result of the interaction between piles and soil [2]. Therefore, the mudcake and pile length-diameter ratio are important factors in changing the friction properties of soil around the pile [3], and it is of great engineering application value to study their effects on the bearing capacity of slurry wall-protected cast-in-place piles.

At present, some scholars have carried out model test, numerical simulation, and field test on the bearing properties of bored piles with the influence of single factor of mudcake or pile length-diameter ratio. Majeed and Haider [4] established the load-settlement curve and predicted the ultimate bearing capacity of bored pile by the Chin-Konder method. Based on artificial neural network (ANN), Wang et al. [5] and Moayedi and Armaghani [6] developed settlement and bearing capacity prediction models of different piles under different behaviors. These models were proved to have high reliability by experiments. Jebur et al. [7] described the effect of pile length-diameter ratio and sand pile friction angle on pile settlement through a new artificial intelligence optimization model algorithm. Chen et al. [8] found that the mudcake concentration will significantly reduce the proportion of pile side resistance of friction pile in sandy cobble stratum by indoor model test. Aleksandar [9] believes that there is an interaction between end resistance and side resistance, and increasing the pile length will strengthen the local effect of pile side resistance. Zhou and Chen [10] found through experiments and PLAXIS simulation that the degree of soil friction degradation was related to the strength and height of the soil around the pile tip. If the strength of the soil around the pile tip was higher, the additional mudcake effect was more serious, and the friction

reduction was greater. If the strength of the soil around the pile tip was lower, the influence of the additional mudcake on the pile side friction was reduced. Based on a numerical model, Zhou et al. [11] found that increasing pile length and diameter is an effective and economical way to improve vertical and lateral bearing capacity. Alielahi and Adampira [12] determine the actual bearing performance of piles by various methods according to the engineering examples. Wang et al. [13] found that the monopile load in the loess area is mainly undertaken by the reaction force provided by the pile lateral friction resistance.

Although scholars have carried out research on the influence of single factors such as mudcake and length-diameter ratio on the bearing characteristics of bored cast-in-place piles, there is little detailed introduction in indoor model tests, especially in the control of mudcake thickness. In summary, the research on the bearing capacity of bored piles under the combined influence of mudcake and pile length-diameter ratio is still insufficient. The test of bearing capacity of piles with mudcake thickness has been done, which was introduced in [14]. This paper focuses on the influence of length-diameter ratio on the bearing capacity of piles with slurry wall protection, and the pile without mudcake around the pile is the control group. Therefore, this paper carried out pile loading tests under different mudcake thicknesses (0 and 0.5 mm) and different length-diameter ratios (10, 14, and 24) via indoor model test and finite element modeling method and analyzed the variation of pile top displacement, pile bearing capacity, axial force, and lateral friction resistance under vertical load, hoping to provide a reference for relevant projects.

2. Indoor Model Test

2.1. Model Pile Preparation

2.1.1. Model Pile. Based on the scale ratio of the model test (1 : 20), the hollow organic glass tube with a diameter of 50 mm is selected for the model pile, and the size of six groups of model piles is shown in Table 1. In order to exclude the influence of other factors on this test, all piles are the same batch of products prepared under the same conditions. After sampling, the elastic modulus test is carried out, and the elastic modulus of the selected samples is determined to be 2.98~3.03 GPa, which is low in dispersion. The error of the test results can be ignored. Therefore, the elastic modulus of the pile is taken as 3 GPa, and the bottom of the pile is sealed with an organic glass. In order to enhance the lateral friction, the pile is uniformly polished with sandpaper. The preparation process of the model pile is shown in Figure 1.

2.1.2. Mudcake. Mudcake is a layer of sticky clay between the pile and the soil on the side of the pile [14]. The mudcake is taken from the site of the second section of the south extension project of a highway in Hefei, and it is evenly brushed on the pile by brush. The fixed water-soil ratio is used to make mudcake so as to ensure that the density of mudcake is basically uniform and avoid the impact of different mudcake densities on the experimental results. Among them, the mudcake density can be obtained by the following methods: First, weigh the mass m_1 of the 100 ml measuring cylinder with an electronic scale with an accuracy of 0.1 g, and then mix the mud retrieved on-site and pour it into the measuring cylinder. Measure the mass m_2 of the measuring cylinder containing 100 ml mud again, and calculate the density of the mud as 1.119 g/cm^3 using formula (1). Since the colloid rate is also an important index to evaluate the drilling mud, the colloid rate of mud selected for this test is determined to be 95.5%.

$$\gamma = \frac{m_2 - m_1}{V_1}, \tag{1}$$

where m_1 is the mass of measuring cylinder; m_2 is the sum of measuring cylinder and mud quality; and V_1 is the volume of mud.

The mudcake preparation process is as follows: the mudcake in the slurry tank is stirred by engineering machinery and equipment, and then the mudcake is taken out and loaded into the bucket. Before each test, the mixer is used to stir it evenly for more than 10 minutes. The thickness of mudcake d is determined by

$$d = \frac{m_4 - m_3}{\gamma L}, \tag{2}$$

where m_3 is the weight of pile; m_4 is the weight of pile and mudcake; γ is the mudcake density; and L is the pile length.

2.2. Model Box and Model Soil

2.2.1. Model Box. To eliminate the influence of the boundary effect on the bearing performance of piles, a circular steel bucket with a diameter of 1200 mm, a height of 1800 mm, and a thickness of 10 mm was used as the model box. Mark the scale in the vertical direction around the model box in advance, transport the model soil in plastic buckets, pack 300 mm high medium sand each time, compact to 260 mm, and repeat this procedure many times. After filling to the specified height, select model soil with a depth of 0 cm, 30 cm, 60 cm, 90 cm, and 120 cm, respectively, by ring knife method for density test, so as to ensure that the compactness of the model soil is consistent, and the final thickness of the soil layer is 1.8 m.

2.2.2. Model Soil. The model soil is medium sand, which is taken from the section project site of Ningbo Rail Transit Line 1; the longitudinal profile of the project is shown in Figure 2. The physical and mechanical parameters of the sand in the model soil shall be determined. The test includes density test, particle gradation analysis test, and direct shear test.

(1) Density Test. The model soil density test is carried out by the ring knife method. The ring knife with a volume of 60 cm^3 is selected. After three measurements, the average value is taken. The measured data are shown in Table 2. The density of model soil is calculated according to the following formula:

Table 1: Groups of piles in the model test.

Number	Mudcake thickness (mm)	Length-diameter ratio	Pile length (mm)	Pile diameter (mm)
M0	0	10	500	50
M1	0.5	10	500	50
M2	0	14	700	50
M3	0.5	14	700	50
M4	0	24	1200	50
M5	0.5	24	1200	50

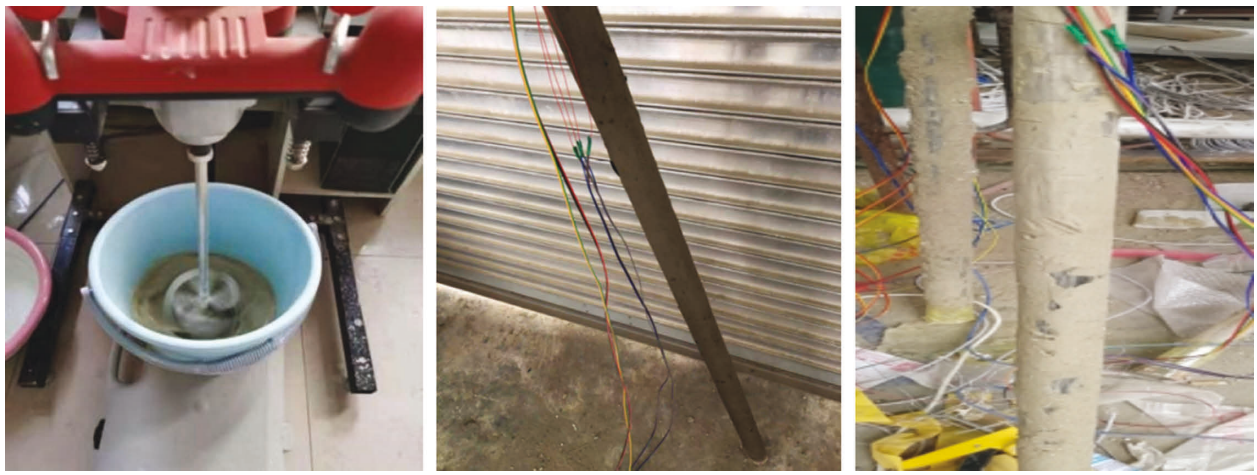

(1) Mixing mudcake before test (2) Test piles after maintenance (3) Slurry wall-protected piles after test

Figure 1: Model piles. (a) Mixing mudcake before test. (b) Test piles after maintenance. (c) Slurry wall-protected piles after test.

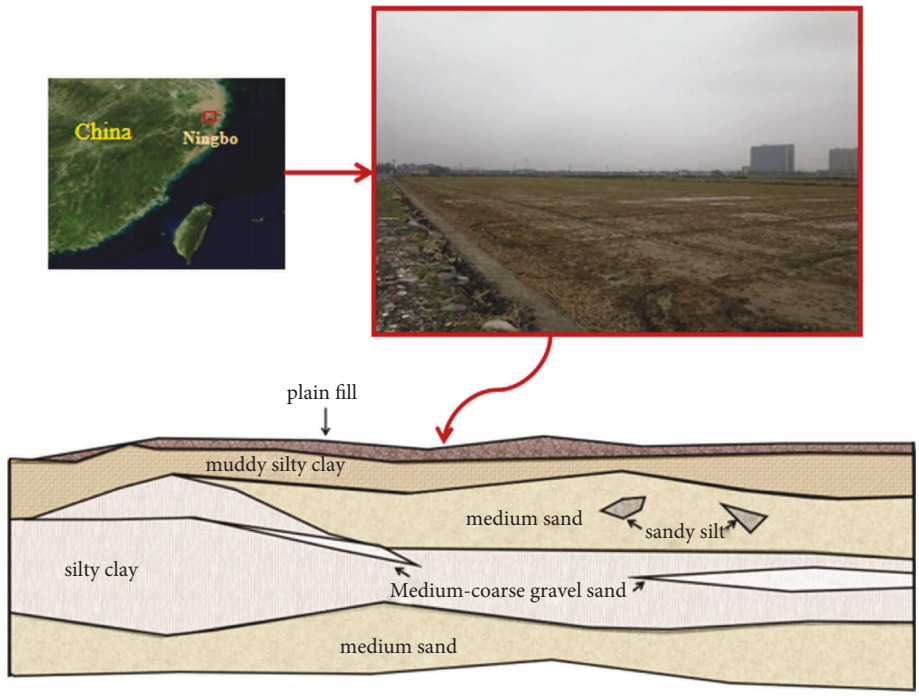

Figure 2: Longitudinal profile of the project.

Table 2: Measured data.

m_6+m_7 (g)	m_5 (g)	Net weight (g)	Volume (cm^3)	ρ_0 (g/cm^3)
318.5	427.12	108.62	60	1.810
318.5	427.98	109.48	60	1.825
318.5	428.01	109.51	60	1.824

Table 3: Screening results.

Pore sizes (mm)	Mass of retained sample (g)	Sample mass less than the pore sizes (g)	Percentage of samples smaller than the aperture in the total sample (g)
2	0	200	100
1.18	21.9	178.1	89.05
0.6	34.2	143.9	71.95
0.3	106.6	37.3	18.65
0.15	22.6	14.7	7.35
0.075	10.7	4	2
—	4	—	—

(a) (b)

Figure 3: Tools for distribution of size. (a) Electronic scales. (b) Sieves of different pore sizes.

$$\rho_0 = \frac{m_5 - m_6 - m_7}{V_2}, \tag{3}$$

where m_5 is the total mass of ring cutter, soil, and base plate; m_6 is the quality of ring cutter; m_7 is the quality of base plate; and V_2 is the volume of ring knife.

Therefore, the tested model soil density is 1.82 g/cm^3.

(2) Particle Grading Test. The model soil is sieved by the sieving method, and the pore sizes of the fine sieves are 2, 1.18, 0.6, 0.3, 0.15, and 0.075 mm, respectively. Take 200 g of model soil with an electronic scale with an accuracy of 0.1 g and shake it for 15 minutes. The screening results are shown in Table 3, and the electronic scale and sieve are shown in Figure 3.

Based on "Test Methods of Soils for Highway Engineering" [15], the percentage of particle mass smaller than a certain particle size in the total soil mass in the sample can be calculated according to

$$X = \frac{a}{b} \times p \times 100, \tag{4}$$

where X is the mass percentage of particles smaller than a certain size, calculated to 0.1%; A is the mass of particles smaller than a certain particle size in the sample passing the 2 mm sieve; B is the mass of the sample taken from the soil sample passing the 2 mm sieve; P is the mass percentage of particles with particle size less than 2 mm.

The nonuniformity coefficient and curvature coefficient can be calculated according to

Figure 4: Direct shear apparatus.

Table 4: Parameters of soil.

Density (g·cm^{-3})	Elastic modulus (MPa)	Poisson ratio	Cohesion (kPa)	Internal friction angle (°)
1.82	50	0.35	0	30

$$C_u = \frac{d_{60}}{d_{10}}, \tag{5}$$

$$C_c = \frac{d_{30}^2}{d_{10}d_{60}}, \tag{6}$$

where C_u is the nonuniformity coefficient; d_{60} is the restricted particle size; d_{10} is the effective particle diameter; C_c is curvature coefficient; d_{30} is a particle size on the particle size distribution curve of soil; and the mass of soil particles smaller than this particle size is 30% of the total mass of soil particles.

Therefore, the coefficient of nonuniformity and coefficient of curvature of the model soil in this test are determined to be 2.94 and 1.69, respectively.

(3) Direct Shear Test. The direct shear test of model soil adopts the fast shear method. Four samples are selected from the model soil and applied with pressures of 100, 200, 300, and 400 kPa in the vertical direction, and the horizontal shear force is applied along the shear plane at a speed of 0.01 mm/min to obtain the shear stress at the time of failure. The displacement value and the corresponding dynamometer reading are recorded every time the shear displacement of the soil sample increases by 0.2 mm until the peak value of the dynamometer reading appears. At this time, the failure value should be recorded, and the direct shear apparatus is shown in Figure 4. Calculate the shear force of model soil according to

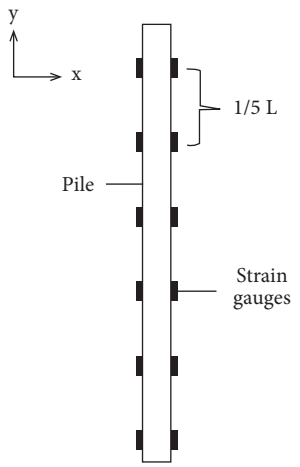

Figure 5: Layout diagram of strain gauge.

$$\tau = \frac{C \cdot R}{A} \cdot 10, \tag{7}$$

where R is the reading of force measuring meter; C is the calibration coefficient of dynamometer; A is the sample area; *10* is the unit conversion factor.

Therefore, the parameters required for the model soil are shown in Table 4.

2.3. Test Device and Loading Scheme. The strain gauge of BE120-3A was selected, and it was symmetrically attached to

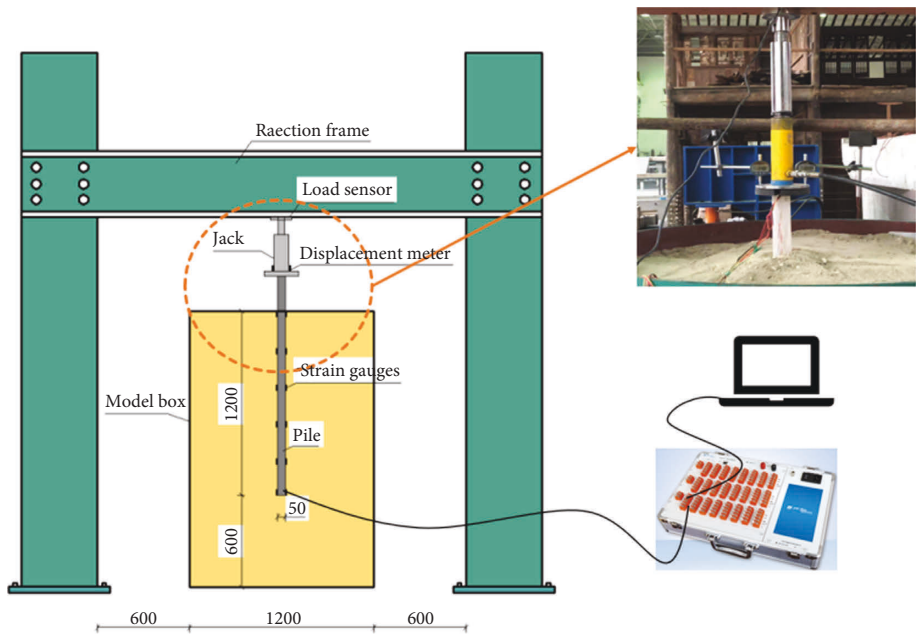

Figure 6: Loading test diagram of model piles (taking 1200 mm pile length as an example).

the front and rear sides of the pile by 502 glue and epoxy resin glue. The vertical spacing of the strain gauge on the same side was 1/5 of the pile length, and the strain gauge was connected to the data collection instrument by the half-bridge method. The data acquisition instrument is connected to the computer by network cable, and then the data are collected and extracted by data processing software. The arrangement of strain gauges is shown in Figure 5.

To better conform to the actual working conditions and protect the mudcake, the pile is arranged by the non-displacement (undisturbed) method, as stated by Azzam and Al Mesmary [16]; that is, the model pile is suspended vertically and centrally to a position 20 cm higher than the bottom of the model box. The sand is poured and compacted by the method in Section 2.2.1 to achieve the target compactness and strictly maintain the consistency of each test installation. The slow maintenance loading mode was used in the model test, and the loading was adopted by the Jack arranged on the pile top. The initial load was 0.5 kN, which was added according to the tolerance of 0.5 kN. The pile top load and displacement were read every 5, 10, 15, 30, 45, and 60 min during the loading. Loading stability criteria and termination conditions are carried out based on "Technical Specification for Building Pile Foundation" [17]. The pile loading device is shown in Figure 6.

3. Analysis of Indoor Model Test Results

3.1. Load-Settlement Analysis. The vertical static load-settlement (Q-s) curve can reflect the load transfer and bearing behavior of the pile-soil system. The load-settlement (Q-s) curves of the six piles are displayed in Figure 7. Based on the "Technical Specification for Building Pile Foundation," the load corresponding to the ultimate displacement $S = 0.06\ D$ is taken as the ultimate bearing capacity of the pile; that is, take the load when the pile settlement is 3 mm. The ultimate bearing capacity of the pile is shown in Table 5.

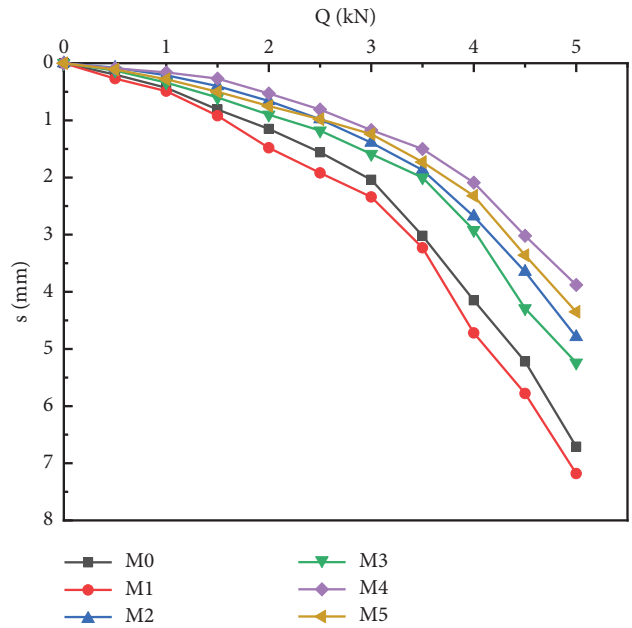

Figure 7: Q-s curve.

Table 5: The ultimate bearing capacity of the model piles.

Pile	M0	M1	M2	M3	M4	M5
Ultimate bearing capacity (kN)	3.49	3.37	4.16	4.03	4.49	4.33

It is not difficult to see from Figure 7 that, under the same vertical load, the settlement of piles without mudcake (M0,

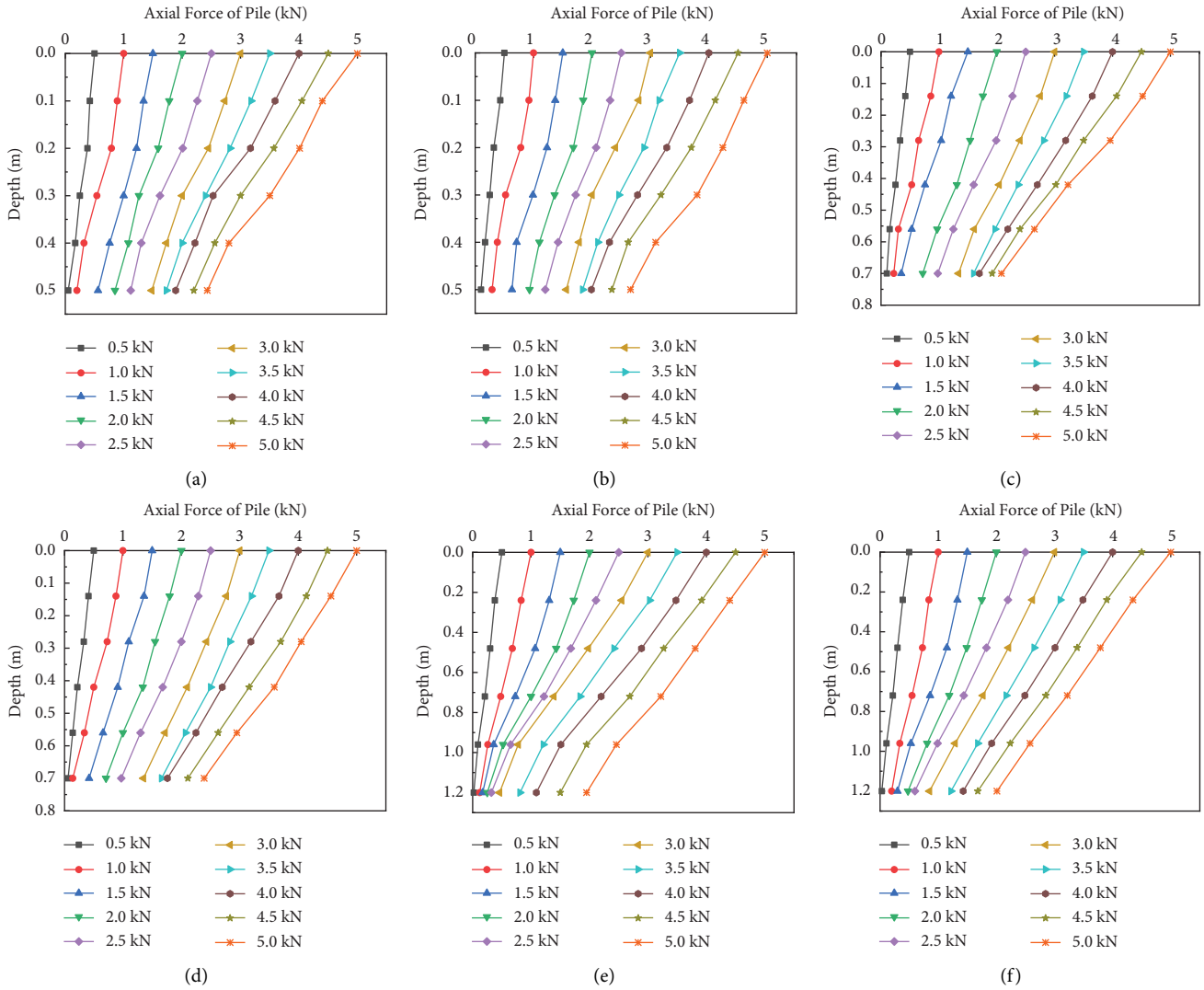

Figure 8: Axial force curves of model piles. (a) M0. (b) M1. (c) M2. (d) M3. (e) M4. (f) M5.

M2, and M4) and piles with mudcake (M1, M3, and M5) decreases with the increase of length-diameter ratio. The settlement of the pile with mudcake is greater than that of the pile without mudcake under the same load and the same pile length, and the larger the length-diameter ratio is, the greater the increase of pile settlement is.

As can be seen from Table 5, the existence of mudcake resulted in the decline of pile bearing capacity. When the length-diameter ratio is 10, 14, and 24, the ultimate bearing capacity of the pile decreases by 0.12 kN, 0.13 kN, and 0.16 kN, respectively. When there is no mudcake (M0, M2, and M4) and mudcake (M1, M3, and M5), the ultimate bearing capacity of every pile increases gradually when the length-diameter ratio is greater, and after reaching the ultimate bearing capacity, the slope of Q-S curve increases significantly, which is consistent with literature [7, 18].

Compared with M0 pile, the ultimate bearing capacity of M2 and M4 piles increased by 19.20% and 15.47%, respectively. Compared with M2 pile, the ultimate bearing capacity of M4 and M5 piles increased by 7.93% and 4.09%, respectively. It shows that when the pile length increases, even if there is mudcake around the pile, the bearing performance can still be improved.

3.2. Analysis of Pile Axial Force. The axial force of the pile section can be derived in accordance with the strain of the pile under each loading stage. The formula is

$$N = \varepsilon_i EA, \tag{8}$$

where E is the elastic modulus of the pile, A is the cross-sectional area of the pile, and ε_i is the strain in the i_{th} section. Figure 8 indicates the variation of the axial force of six piles when different loads are applied.

It can be perceived from Figure 8 that the axial force curve is nonlinearly distributed, and the slope change of the curve represents the trend of the lateral friction of the monopile, as stated by Sang [19]. The larger the slope is, the smaller the lateral friction is. Under the action of vertical load, the pile body is gradually compressed, and the relative

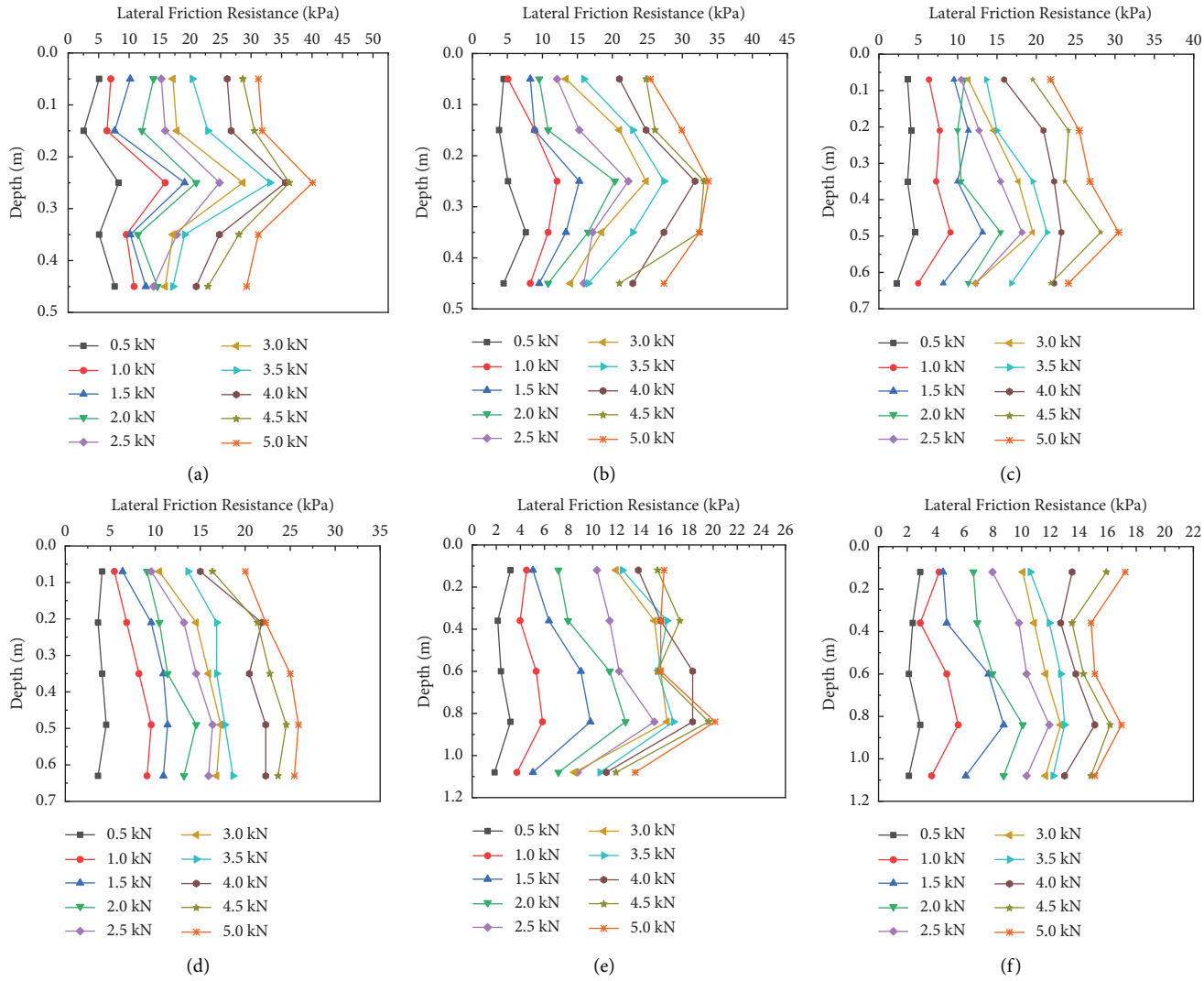

Figure 9: Lateral friction resistance curves of model piles. (a) M0. (b) M1. (c) M2. (d) M3. (e) M4. (f) M5.

displacement between the pile body and the pile side soil is generated. At this time, the lateral friction resistance of the pile side soil begins to play a role. The overall trend is as follows: under the same pile vertical load, the axial force decreases gradually with the increase of the buried depth of the pile, and the maximum axial force is at the pile top. At the same depth relative to the pile top, the axial force of the pile is positively correlated with the pile vertical load. The greater the vertical load on the top of the pile, the greater the pile axial force at the same position, so it belongs to the friction end-bearing pile. It can also be seen from Figure 8 that when the upper load is small, the lower axial force of the pile with a large length-diameter ratio is smaller or even tends to be 0. By comparing the axial force curves of piles M0 and M1, M2 and M3, and M4 and M5, it is found that the thickness of mudcake has a significant effect on the ratio of tip resistance to pile vertical load. This is because the mud around the pile reduces the friction coefficient between the pile and soil, thereby weakening the exertion of the pile lateral friction resistance.

3.3. Analysis of Pile Lateral Friction Resistance. Pile lateral friction could be derived from the axial force, and the average lateral friction in paragraph i is

$$q_{si} = \frac{N_i - N_{i+1}}{A_i}, \tag{9}$$

where A_i is the upper and lower sections between the pile side surface area and N_i and N_{i+1} are the axial force in the i_{th} and $(i+1)_{th}$ sections, respectively.

Figure 9 shows that when the vertical load on the pile top is small, with the increase of the buried depth of the pile, the lateral friction curve of the pile increases from small to maximum and then gradually decreases. At the same depth, the pile lateral friction is positively correlated with the pile vertical load, and the overall distribution is "hump." The greater the pile vertical load, the better the lateral resistance. With the increasing load applied on the pile top, the stress center of lateral friction gradually shifts from the upper part of the pile to the lower part of the pile; that is, the pile lateral resistance in different depths of the soil layer is

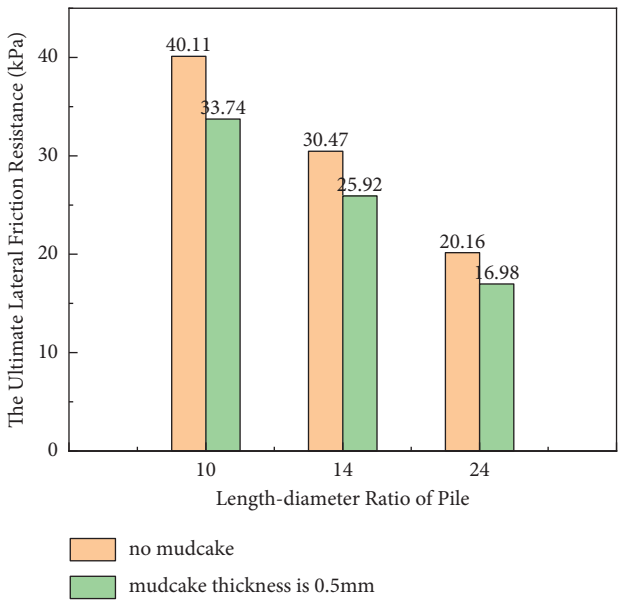

Figure 10: The diagram of the relationship between ultimate lateral friction resistance and length-diameter ratio.

asynchronously exerted. The farther the distance to the pile top is, the slower the pile lateral resistance is exerted. With the increase of the length-diameter ratio, the farther peak position is from the pile top because the lateral Earth pressure of the upper soil on the pile is small, so the lateral resistance is small.

Because of the small axial force of the lower pile, the relative displacement generated by the soil around the pile is reduced, and the lateral resistance at the pile end is also weak. As shown in Figure 10, when the length of the pile is the same, the ultimate lateral friction resistance of the pile with mud defect will also be reduced. Compared with the pile without mud defect with an aspect ratio of 10, 14, and 24, the ultimate lateral friction resistance of the pile with mud defect will decrease by 15.89%, 14.93%, and 15.77%, respectively. For the mud wall-protected cast-in-place pile, the length-diameter ratio has a more significant effect on the reduction of the ultimate lateral friction of the pile. The ultimate lateral friction of the pile with the length-diameter ratio of 14 and 24 decreases by 23.2% and 48.9%, respectively, compared with the pile with the length-diameter ratio of 10.

3.4. Characteristics of Pile Tip Resistance. The change trend of pile tip resistance is shown in Figures 11 and 12. The relationship between pile tip resistance and pile vertical load curve is nonlinear. When the pile vertical load is small, the pile tip resistance almost plays no role. With the increase of load, the pile tip resistance gradually comes into play, and the curve change rate gradually accelerates. The smaller the length-diameter ratio, the greater the proportion of tip resistance and the steeper the curve. This is because the pile lateral friction of large length-diameter ratio pile is longer, and the load is mainly borne by the pile lateral friction. The existence of mudcake will affect the

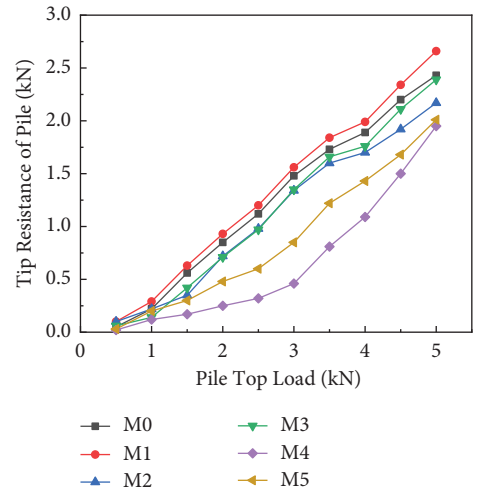

Figure 11: Curve of tip resistance and vertical load.

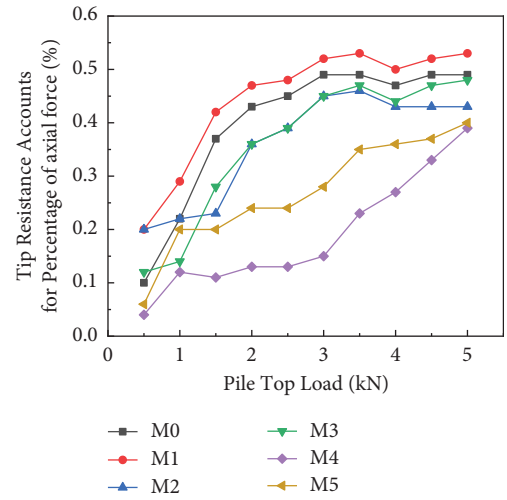

Figure 12: Relation curves between the tip resistance account for the percentage of axial force and pile top load.

friction coefficient of the pile side and reduce the pile lateral friction resistance, but the length-diameter ratio will restrict the adverse effect of mudcake on the tip resistance.

4. Analysis of Numerical Simulation

4.1. Establishment of the Numerical Model. The size and parameter setting of pile and soil are consistent with the indoor model test. The diameter of the pile is 50 mm, the length is 500 mm, 700 mm, and 1200 mm, the diameter of soil around the pile is 1200 mm, and the height is 1800 mm. The material parameters are shown in Table 6.

Although the two-dimensional axisymmetric analysis can simplify the program and obtain the results more easily in a short time, in order to facilitate the comparison with the pile group work carried out in the future, the three-dimensional model is used for analysis in this paper. The pile is modeled by the linear elastic model, and the soil and mudcake are modeled by the Mohr–Coulomb model. The

Table 6: Model material parameters.

Materials	Elastic modulus (MPa)	Poisson ratio	Friction angle (°)	Cohesion (kPa)
Soil	50	0.35	30	0
Pile	3000	0.25		
Mudcake	10	0.35	10	10

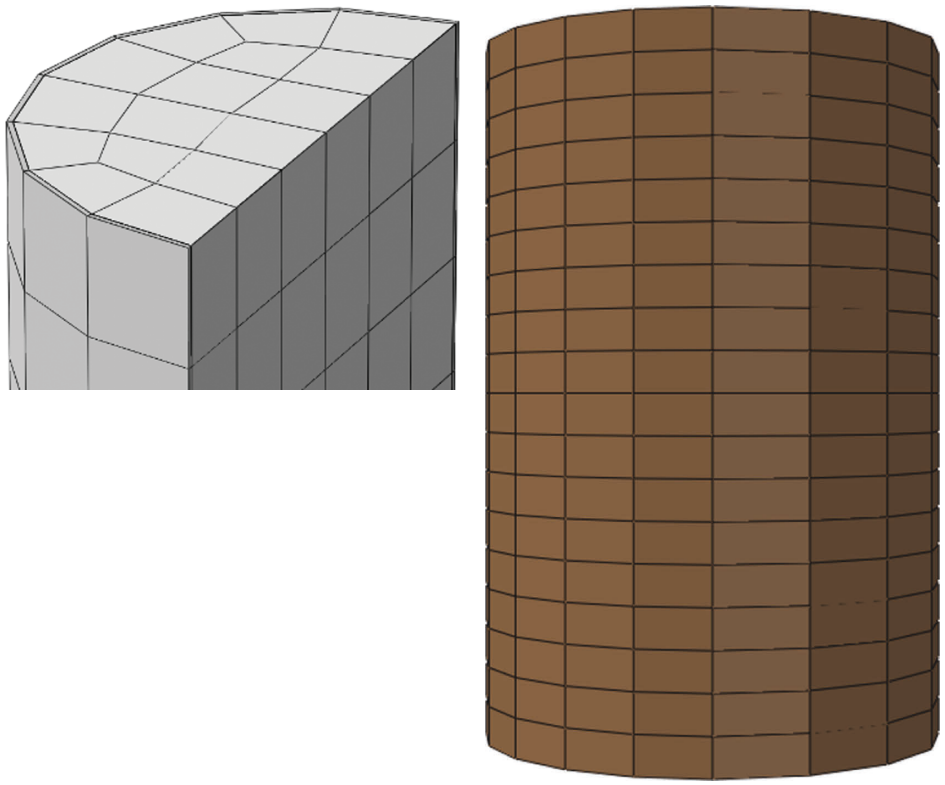

(a) (b)

Figure 13: Grid graph of S1 pile. (a) Pile and mudcake. (b) Soil.

model is mainly applicable to materials characterized by particle structure under monotonic loading [20]. The pile-muddy-soil contact surface adopts a master-slave contact relationship, the friction coefficient is set as $\tan 30° = 0.57$, and the normal is set to hard contact. The tie-binding constraints are selected between the pile bottom and the soil top. The model adopts C3D8 elements, and the grid type is hexahedral. The relevant setting parameters refer to [21]. The grid division of S1 pile is shown in Figure 13. After many times of simulation analysis, it is found that the mesh size of the current model can better meet the requirements of calculation accuracy and running time, so the subsequent models use this mesh density as the optimal mesh density to carry out simulation calculation. After setting the initial stress, the stress balance is realized in the analysis step. Then, the pile element is activated to make it in contact with the surrounding soil. Since the pile weight is larger than the soil weight, the stress state is slightly changed. This approach is suitable for the installation process of bored piles [22]. From the top of the pile, vertical downward loading is divided into 10 stages, the first stage of loading is 0.5 kN, and then each stage increases by 0.5 kN until 5 kN.

It should be underlined that the installation effect of the pile will affect the stiffness of the soil by changing the stress state around the pile, which further leads to a significant change in the bearing capacity of the pile over time [23–25]. However, because this paper focuses on the influence of different length-diameter ratios on the bearing capacity of the pile and has strictly maintained the consistency of each test installation method, this paper does not consider the specific impact of the installation effect on the bearing capacity of the pile.

4.2. Load-Settlement Analysis. It should be noted that the coding of the simulation piles is parallel to the test piles and that the same numbered piles have the same features. It can be inferred from Figures 14 and 15 and Table 7 that the simulated settlement curve is slowly changing without an obvious inflection point. When the vertical load is small, the settlement of piles with different length-diameter ratios is small, and the difference is not obvious. As the length-diameter ratio increases, the settlement difference between the control group with the same pile length and the pile with

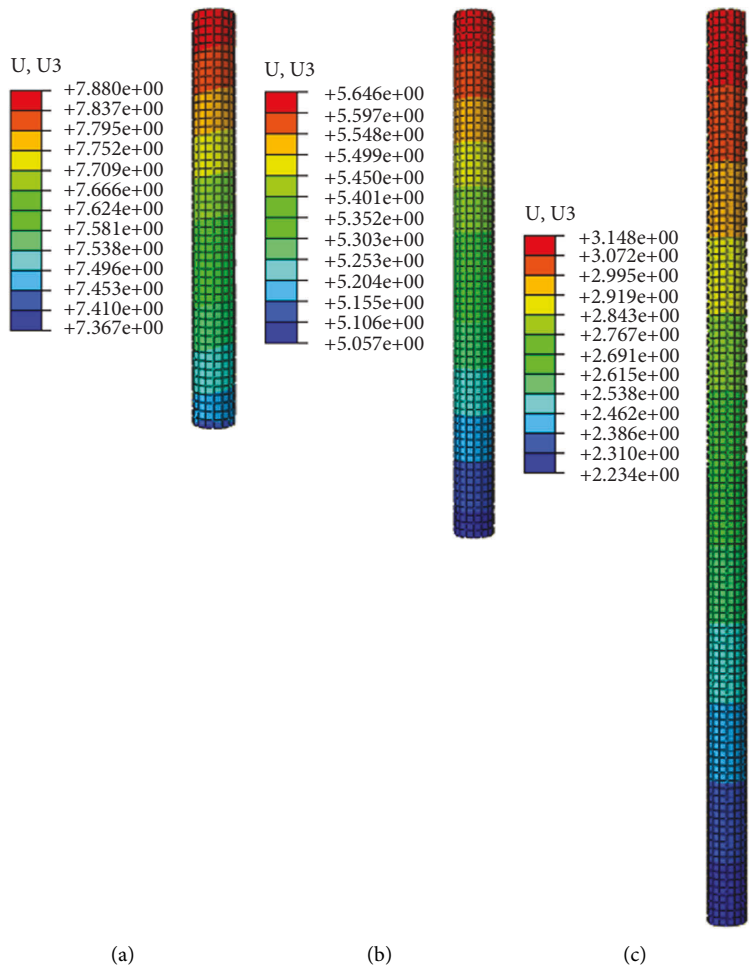

Figure 14: Settlement of simulation piles with different length-diameter ratios (unit: m). (a) S1. (b) S3. (c) S5.

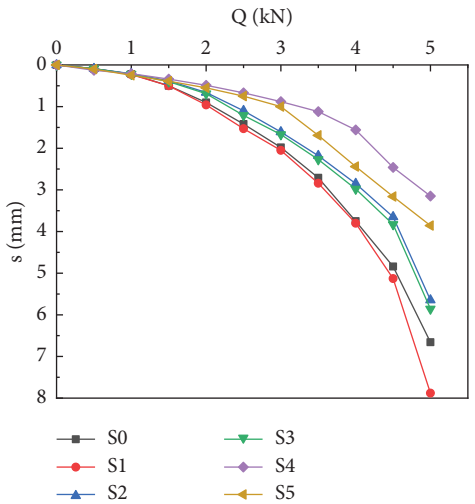

Figure 15: Q-s curves.

mudcake gradually appears, indicating that the lubrication effect of mudcake will be more obvious as the length-diameter ratio increases. The ultimate bearing capacity of pile is positively correlated with the length-diameter ratio; that is,

Table 7: The ultimate bearing capacity of simulation piles.

Pile	S0	S1	S2	S3	S4	S5
Ultimate bearing capacity (kN)	3.81	3.64	4.09	4.03	4.89	4.81

the larger the length-diameter ratio is, the better the bearing capacity of monopile is. Under the same vertical load, the settlement of pile decreases with the increase of length-diameter ratio, and the Q-s curve is more stable. Therefore, the pile with a large length-diameter ratio has a more obvious effect on controlling settlement.

As the finite element software is too idealistic to deal with the process of pile-soil interaction, there will be some differences between the numerical values of the model test and the finite element model under the same influence factors. By comparing the data in Tables 5 and 7, the settlement of every simulated pile is slightly larger than that of the test pile, but the variation laws obtained by the two are basically the same; that is, the mudcake on the pile side will increase the settlement of the pile top and weaken the ultimate bearing capacity of the pile. The larger the length-diameter ratio is, the smaller the settlement of the pile is, the smaller the proportion of the load borne by the soil is, and the greater

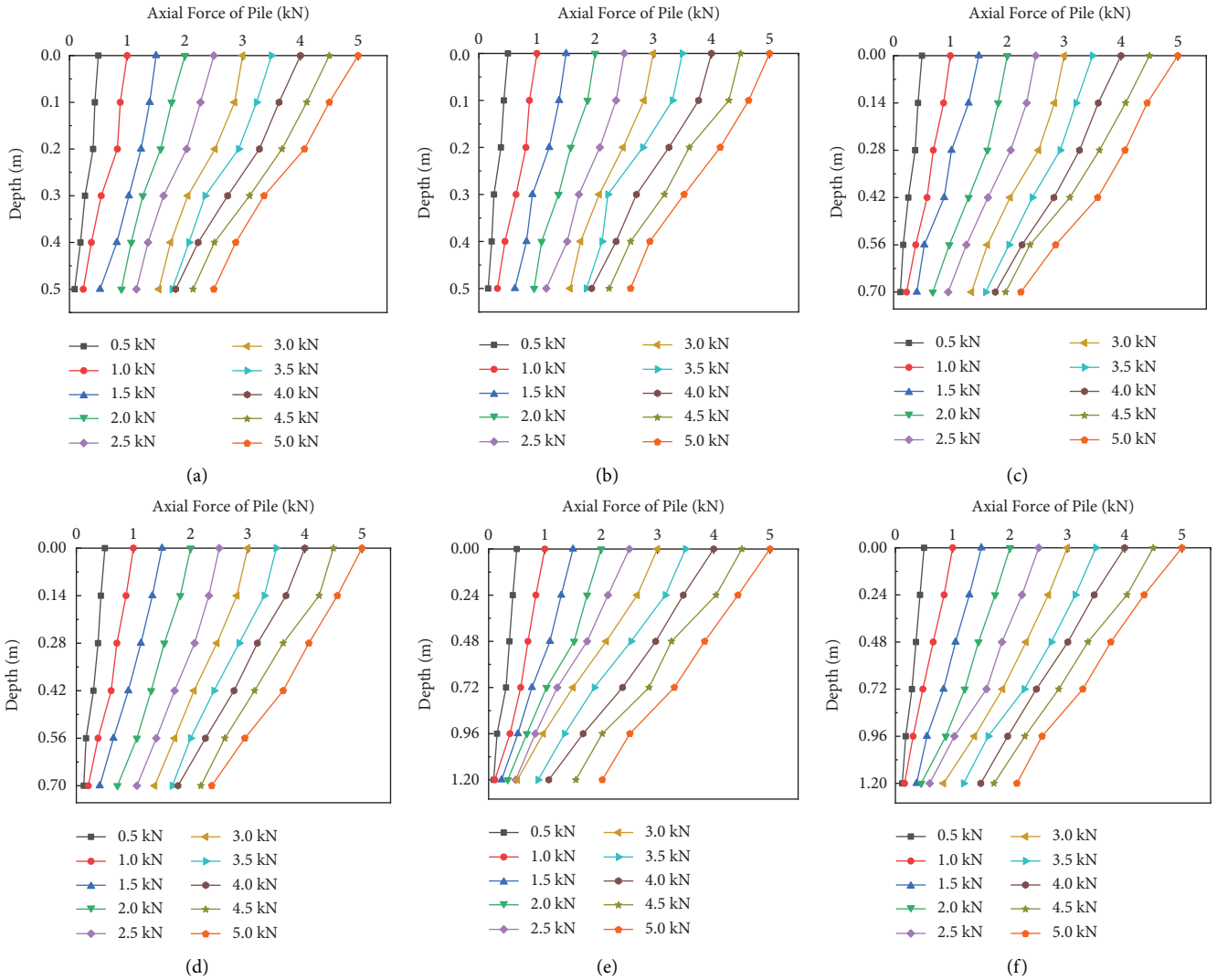

Figure 16: Axial force curves of simulation piles. (a) S0. (b) S1. (c) S2. (d) S3. (e) S4. (f) S5.

the ultimate bearing capacity is. Compared to the bored pile with the length-diameter ratio of 10, the ultimate bearing capacity of the bored pile with the aspect ratio of 24 increases by about 30%.

4.3. Analysis of Pile Axial Force. The pile axial force curve is displayed in Figure 16. There is a nonlinear relationship between the pile axial force and depth, which is basically in accordance with the change tendency of the axial force of the model test. The larger the aspect ratio is, the smaller the axial force is. The maximum axial force is located at the top of the pile and gradually decreases along the pile. Mudcake around pile will reduce the friction factor between soil and pile and improve the bearing ratio of pile tip resistance to the pile ultimate bearing capacity.

4.4. Characteristics of Pile Tip Resistance and Axial Force. The change tendency of tip resistance of modeling piles is displayed in Figures 17 and 18. The smaller the length-

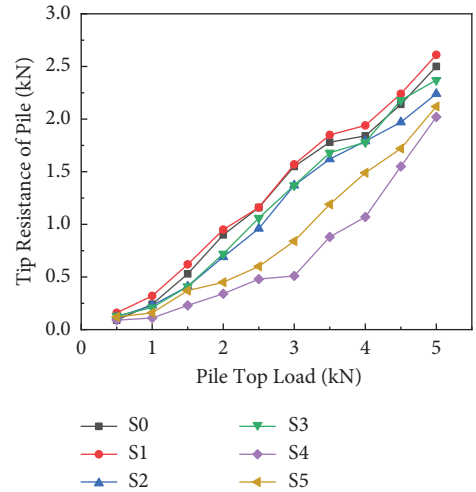

Figure 17: Curve of pile tip resistance and pile top load.

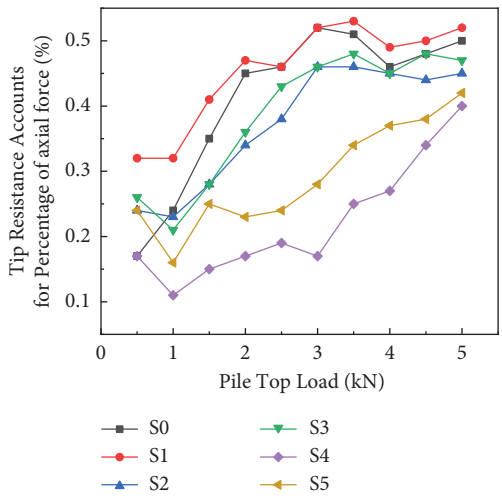

Figure 18: Relation curves between the tip resistance account for the percentage of axial force and pile top load.

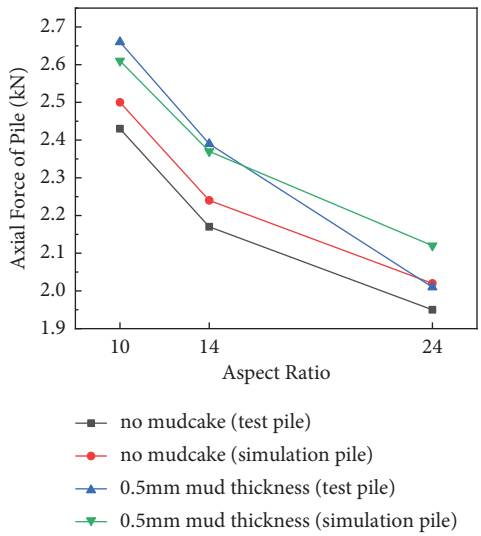

Figure 19: Curve of pile tip resistance and length-diameter ratio.

diameter ratio is, the larger the proportion of tip resistance is, and the mud effect has a more obvious effect on the proportionality of tip resistance to pile vertical load. Under the load of 5 kN, the resistance of S1 pile tip is 2.61 kN with a proportion of 0.522, the resistance of S3 pile tip is 2.37 kN with a proportion of 0.474, and the resistance of S5 pile tip is 2.12 kN with a proportion of 0.424.

Combined with the above analysis, it can be inferred that the settlement law and axial force change trend of model test and numerical simulation are generally consistent. The settlement of the pile is inversely correlated with the aspect ratio and positively associated with the thickness of mudcake. The effect of the length-diameter ratio on the displacement of pile is significantly greater than the effect of mudcake on the displacement of pile, and the ultimate lateral friction and pile tip resistance are significantly reduced as the length-diameter ratio increases.

Under the 5 kN load, the axial force of the control group (S0, S2, and S4) and mudcake thickness of 0.5 mm pile (S1, S3, and S5), as shown in Figure 19, showed that, under the same load, simulation pile and model pile tip resistance have the same tendency along with the change of length-diameter ratio, that is, the simulation results are basically reliable. The axial force of pile tip is negatively correlated with the length-diameter ratio. Its decreasing rate decreases gradually as the pile length-diameter ratio increases. The axial force of pile tip increases with the increase of mudcake thickness, but the increasing effect of mudcake thickness on the axial force of pile tip is not enough to compensate for the weakening effect of length-diameter ratio on the axial force of pile tip.

5. Conclusion

According to the results of the indoor model test and numerical simulation of six bored piles, it is inferred that the influence of mudcake and length-diameter ratio on the bearing performance of piles is mutual influence, and the following conclusions are obtained:

(1) With the increase of length-diameter ratio, the lubrication effect of mudcake will become more obvious, which makes the settlement difference between the control group and the bored pile of the same length gradually appear, and the bearing ratio of tip resistance to the ultimate bearing capacity continuously increases.

(2) The axial force of pile tip has a negative correlation with the length-diameter ratio and positive association with the thickness of the mudcake. However, the influence of the mudcake thickness on the axial force of pile tip is still insufficient to compensate for the weakening effect of the length-diameter ratio on the axial force at the pile end.

(3) For the bored piles, the increase of the length-diameter ratio will induce the increase of the proportion of pile lateral friction resistance and the decrease of the ultimate lateral friction resistance. For the cast-in-place piles with length-diameter ratios of 14 and 24, the ultimate pile friction resistance is 23.2% and 48.9% lower than that of piles with a length-diameter ratio of 10, respectively.

At present, this paper only studies the bearing behavior of single pile with different length-diameter ratios, and the bearing characteristics and settlement law of pile groups under different length-diameter ratios will be subject to relevant model tests and numerical simulation analysis in the future. Overall, the larger the length-diameter ratio of the bored pile is, the more effectively it can restrain the adverse effects of mudcake on pile settlement and end resistance and then improve the bearing performance of the pile. However, it is not that the larger the length-diameter ratio is, the better it is. Therefore, in order to give full play to the soil friction in practical engineering, the thickness of the mudcake around the pile must be strictly controlled while selecting the optimal pile length.

Data Availability

The data used to support the findings of this study are included within the article.

Conflicts of Interest

No potential conflicts of interest were reported by the authors regarding the publication of this paper.

Acknowledgments

This study was funded by the Scientific Research Project of Anhui Jianzhu University (no. 2019QDZ24).

References

[1] X. Wang, Y. Yang, R. Yang, and P. Liu, "Experimental analysis of bearing capacity of basalt fiber reinforced concrete short columns under axial compression," *Coatings*, vol. 12, no. 5, p. 654, 2022.

[2] G. G. Meyerhof, "Bearing capacity and settlement of pile foundations," *Journal of the Geotechnical Engineering Division*, vol. 102, no. 3, pp. 197–228, 1976.

[3] Z. M. Zhang, J. Yu, G. X. Zhang, and X. M. Zhou, "Test study on the characteristics of mudcakes and in situ soils around bored piles," *Canadian Geotechnical Journal*, vol. 46, no. 3, pp. 241–255, 2009.

[4] A. Majeed and O. Haider, "Simulation of bearing capacity of bored piles," *MATEC Web of Conferences*, vol. 162, p. 01004, 2018.

[5] B. Wang, H. Moayedi, H. Nguyen, L. K. Foong, and A. S. A. Rashid, "Feasibility of a novel predictive technique based on artificial neural network optimized with particle swarm optimization estimating pullout bearing capacity of helical piles," *Engineering with Computers*, vol. 36, no. 4, pp. 1315–1324, 2020.

[6] H. Moayedi and D. Jahed Armaghani, "Optimizing an ANN model with ICA for estimating bearing capacity of driven pile in cohesionless soil," *Engineering with Computers*, vol. 34, no. 2, pp. 347–356, 2018.

[7] A. A. Jebur, W. Atherton, and R. M. Al Khaddar, "Feasibility of an evolutionary artificial intelligence (AI) scheme for modelling of load settlement response of concrete piles embedded in cohesionless soil," *Ships and Offshore Structures*, vol. 13, no. 7, pp. 705–718, 2018.

[8] Y. Q. Chen, J. S. Lei, and L. Xu, "Model test study on influence of mudcake on friction performance of pouring pile," *Journal of Railway Science and Engineering*, vol. 16, no. 07, pp. 1660–1665, 2019, (in Chinese).

[9] S. V. Aleksandar, "Load transfer in pile-soil system," *Translation of Foundation and Foundation, Episode 5, Pile Foundation*, China Architecture and Building Press, Beijing, 1982.

[10] H. B. Zhou and Z. C. Chen, "Analysis of effect of different construction methods of piles on the end effect on skin friction of piles," *Frontiers of Architecture and Civil Engineering in China*, vol. 1, no. 4, pp. 458–463, 2007.

[11] J. Zhou, X. Huang, J. Yuan, J. Zhang, and X. Wang, "Comparative study on the influence of pile length and diameter on bearing capacity and efficiency of root piles, straight-shaft piles and pedestal piles," *Arabian Journal for Science and Engineering*, vol. 46, no. 11, pp. 10439–10456, 2021.

[12] H. Alielahi and M. Adampira, "Comparison between empirical and experimental ultimate bearing capacity of bored piles-a case study," *Arabian Journal of Geosciences*, vol. 9, no. 1, p. 78, 2016.

[13] J. X. Wang, B. W. Zhang, and Y. Yang, "Experimental study on vertical bearing capacity of pile foundation in east Gansu Province loess area," *IOP Conference Series: Earth and Environmental Science*, vol. 525, no. 1, Article ID 012082, 2020.

[14] Z. G. Zhang, J. Cui, M. Y. Ma, and P. S. Xi, "Model test and numerical simulation of the mudcake thickness effect on the bearing capacity of vertically loaded single piles," *Mathematical Problems in Engineering*, vol. 2020, Article ID 5012427, 11 pages, 2020.

[15] "Test methods of soils for highway engineering," *JTG 3430-2020 Test Methods Of Soils For Highway Engineering*, China Communications Press, Beijing, 2020, (in Chinese).

[16] W. R. Azzam and M. Al Mesmary, "The behavior of single tension pile subjected to surcharge loading," *NED University Journal of Research*, vol. 7, no. 1, pp. 1–12, 2010.

[17] "Technical specification for building pile foundation," *JGJ94-2018 Technical Specification for Building Pile Foundation*, China Architecture and Building Press, Beijing, 2018, (in Chinese).

[18] J. Y. Mei, Y. S. Deng, and H. Wang, "Research on model test for vertical bearing capacity of super-long pile," *Building Structure*, vol. 47, no. S2, pp. 464–468, 2017, (in Chinese).

[19] W. F. Sang, "Experiment on bearing capacity of large-diameter and super-long bored pile under vertical heavy load," *Global Geology*, vol. 39, no. 1, pp. 127–134, 2020, (in Chinese).

[20] M. Wehnert and P. A. Vermeer, "Numerical analyses of load tests on bored piles," *Numerical Methods in Geomechanics–NUMOG IX*, pp. 505–511, 2004.

[21] M. J. Xu, P. P. Ni, G. X. Mei, and Y. L. Zhao, "Load-settlement behaviour of bored piles with loose sediments at the pile tip: experimental, numerical and analytical study," *Computers and Geotechnics*, vol. 102, pp. 92–101, 2018.

[22] N. T. V. Phuong, A. van Tol, A. Elkadi, and A. Rohe, "Numerical investigation of pile installation effects in sand using material point method," *Computers and Geotechnics*, vol. 73, pp. 58–71, 2016.

[23] M. Baca, A. L. Ivannikov, and J. Rybak, "Numerical modelling of various aspects of pipe pile static load test," *Energies*, vol. 14, no. 24, p. 8598, 2021.

[24] M. Baca and W. Brzakala, "Numerical modeling of pile installation influence on surrounding soil," *International Multidisciplinary Scientific GeoConference: SGEM*, vol. 17, no. 2, pp. 619–626, 2017.

[25] K. Fakharian and M. Khanmohammadi, "Numerical modeling of pile installation effects on stress state in clay," *Japanese Geotechnical Society Special Publication*, vol. 2, no. 39, pp. 1402–1406, 2016.